ANNUAL REVIEWS

Annual Review of Condensed Matter Physics

The Physics of Dense Suspensions

Christopher Ness,[1] Ryohei Seto,[2,3,4] and Romain Mari[5]

[1]School of Engineering, University of Edinburgh, Edinburgh, United Kingdom; email: chris.ness@ed.ac.uk

[2]Wenzhou Institute, University of Chinese Academy of Sciences, Wenzhou, Zhejiang, China; email: seto@ucas.ac.cn

[3]Oujiang Laboratory, Wenzhou, Zhejiang, China

[4]Graduate School of Information Science, University of Hyogo, Kobe, Japan

[5]Université Grenoble Alpes, CNRS, Laboratoire Interdisciplinaire de Physique (LIPhy), Grenoble, France; email: romain.mari@univ-grenoble-alpes.fr

Annu. Rev. Condens. Matter Phys. 2022. 13:97–117

The *Annual Review of Condensed Matter Physics* is online at conmatphys.annualreviews.org

https://doi.org/10.1146/annurev-conmatphys-031620-105938

Keywords

soft matter, rheology, non-Newtonian fluids, jamming

Abstract

Dense suspensions of particles are relevant to many applications and are a key platform for developing a fundamental physics of out-of-equilibrium systems. They present challenging flow properties, apparently turning from liquid to solid upon small changes in composition or, intriguingly, in the driving forces applied to them. The emergent physics close to the ubiquitous jamming transition (and to some extent the glass and gelation transitions) provides common principles with which to achieve a consistent interpretation of a vast set of phenomena reported in the literature. In light of this, we review the current state of understanding regarding the relation between the physics at the particle scale and the rheology at the macroscopic scale. We further show how this perspective opens new avenues for the development of continuum models for dense suspensions.

1. INTRODUCTION

Suspensions of particles in liquid are found throughout nature and industry, with examples ranging from mud, magma, and blood to cement, paint, and molten chocolate. Often solid and fluid are mixed in roughly equal proportion, leading to a thick or pasty consistency (see **Figure 1*a***). The widespread use of these dense suspensions is enabled by extensive experimental characterization and empirical modeling of their mechanical behavior, or rheology, allowing one to estimate, e.g., the thickness of a poured coating, the energy required to stir a slurry, or the extent of a mudslide. Nonetheless, there are so far no accepted continuum theories; we have not yet identified the dense suspension analog of the Navier–Stokes equations. Doing so requires us to understand the relationship between composition and material properties, that is, to develop a physics of suspensions.

This effort has a rich and extensive history, dating back at least to Einstein (1). The physics of suspensions has long been seen primarily as a fluid mechanical problem, in which the dynamics are dominated by viscous stresses induced by the presence of particles. This perspective led to Batchelor's (2) successful theory for dilute suspensions of solid volume fraction $\phi \lesssim 0.1$. More concentrated suspensions, however, display behaviors that have proven elusive to the fluid mechanical approach, in particular their tendency to transition reversibly from liquid to solid depending on the applied stress. Ketchup, for instance, will only flow out of the bottle under large stresses, whereas cornstarch suspensions (cf. Dr. Seuss's Oobleck) will only flow smoothly under small stresses.

The reminiscence of phase transitions motivated the development of near-equilibrium statistical mechanics approaches (notably mode-coupling theory) to some of these problems in the 2000s, often attributing the emergence of solidity to a glass transition (see, for instance, Reference 3). While this approach proved a powerful tool for colloidal suspensions, in many cases the particles are too large to be significantly influenced by Brownian motion; these suspensions are far from equilibrium. More recently, researchers started to explore an analogy between dense suspensions and dry granular materials, which at the macroscopic scale led to a highly influential constitutive law, the $\mu(J)$ rheology (4). This further triggered intense interest in the microscopic parallels between these two materials, particularly in the role of particle contact forces and associated friction in the stress of dense granular suspensions. The present review centers mostly on the recent developments of this approach, and how a coherent physics of dense suspensions

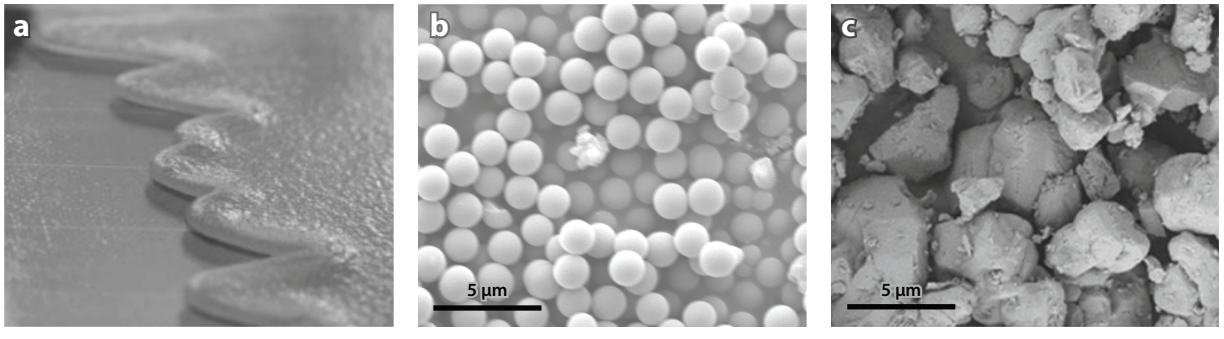

Figure 1

Dense suspensions. (*a*) A particle-laden film comprising 250 μm–450 μm glass beads in glycerol. (*b*) A model system of 1.4 μm monodisperse silica spheres. (*c*) Calcium carbonate particles of approximately 5 μm, with irregular shape. Panel *a* adapted with permission from Reference 9; copyright 2005 American Physical Society. Panel *b* adapted with permission from Reference 10; copyright 2018 The Society of Rheology. Panel *c* adapted with permission from Reference 11; copyright 2017 Rheologica Acta.

is emerging from it. As we discuss below, the rheology of a dense suspension is intimately linked to an underlying out-of-equilibrium transition known as jamming, which occurs when the solid volume fraction ϕ reaches a critical value ϕ_J. By accounting for the proximity of ϕ to this critical value, which, crucially, is stress dependent through many aspects of particle-level physics, one can understand broad spectra of rheology in a consistent way.

Dense suspensions are a mainstay of soft matter science: Understanding their physics is crucial in many industrial settings and is of fundamental relevance. This (necessarily short and incomplete) review aims to equip the reader with an intuitive starting point from which to tackle the vast and varied physics of dense suspensions. Each of the topics covered deserves its own detailed review—indeed many of these have been written and will be cited (see, e.g., 5–8). In what follows, we first outline the pertinent features of dense suspensions. We then introduce jamming in Section 3, before discussing in Section 4 how the macroscopic rheology is governed by microscopic physics that sets the proximity to the transition. In Section 5, we show how microscopic physics can be encoded in continuum models and then introduce some aspects of the fluid mechanics of dense suspensions.

2. WHAT ARE DENSE SUSPENSIONS?

Dense suspensions represent a large subset of complex fluids and can vary considerably in their physical and chemical composition. Here, we briefly list the main sources of physical variability and the characteristics that make a comprehensive description of their physics challenging.

2.1. The Particles

The particles may be stiff solids of arbitrary shape (see **Figure 1*b*,*c***) with crystalline or amorphous structure, or they may instead be soft materials such as hydrogel particles or red blood cells. We focus here on particles that can, to a first approximation, be considered rigid (**Figure 2*a***). Although there are no strict bounds on the particle size a, we restrict the discussion to $\mathcal{O}(100)\,\text{nm} \lesssim a \lesssim \mathcal{O}(1)\,\text{mm}$. Such particles are orders of magnitude larger than their molecular constituents and can, in principle, be characterized using continuum mechanics concepts such as their Young modulus. Crucially, though, they are usually not macroscopic bodies, and nanometer-scale physics remains relevant. The marriage of macroscopic and microscopic physics distinguishes their interactions from those between molecules.

Surface effects in particular play a major role in the interactions between particles (12). Often surfaces are "dressed," either by adsorbed molecules such as polymer brushes or by ion–counterion double layers, providing repulsion (**Figure 2*b***) at length scales typically in the nanometer to micrometer range (5). At this scale surface roughness is also present, as are Van der Waals forces (5). The former may allow the lubrication singularity to be violated; the latter may introduce particle attraction (**Figure 2*c***). To complicate matters further, concepts from the physics of dry granular contacts, for instance, friction (**Figure 2*d***), adhesion, and force chains (13; **Figure 2*e***), appear relevant (14). Sliding friction in particular has been observed at particle level in systems varying considerably in their composition (15, 16), though its origin may differ from that between macroscopic bodies. In both cases, surface morphology probably plays a central role, but whereas for large bodies this creates multicontact interfaces with statistics leading to Amontons–Coulomb law (17), for small particles contact through one or few asperities may be the norm (dependent on the extent of contact deformation), giving rise to load-weakening friction (18, 19). Combining all of these effects, the situation is sufficiently complex that there are no established force models applicable across the size range of interest: Understanding how particles interact is a challenge.

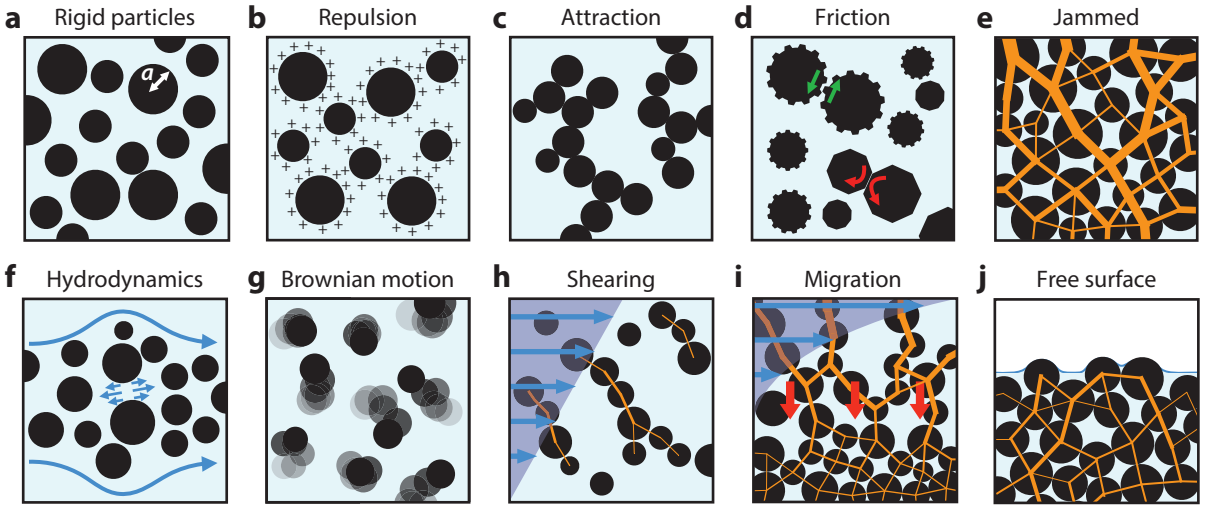

Figure 2

Schematics of dense suspension microphysics. (*a*) A suspension of rigid particles; (*b*) repulsive interactions; (*c*) attractive interactions; (*d*) particle–particle friction, showing inhibited sliding (rough particles highlighting surface asperities, *green arrows*) and inhibited rolling (faceted particles, *red arrows*); (*e*) a jammed state (force chains in *orange*); (*f*) hydrodynamics, showing lubrication (*short arrows*) and drag (*long arrows*); (*g*) Brownian motion; (*h*) shear-induced structure showing particle contact forces (*orange lines*) under a shear flow (streaming velocity shown in *blue arrows*); (*i*) particle migration (*red arrows*) under a shear rate gradient (*blue arrows*) with a gradient in the magnitude of particle contact forces (*orange lines*); and (*j*) free surface, showing curvature of the interface on the scale of the particle size a, leading to capillary forces.

2.2. The Fluid

The fluid, or solvent, is the main factor differentiating suspensions from dry granular media. It mediates hydrodynamic interactions (**Figure 2*f***) and can be a simple liquid (e.g., water), a polymeric fluid (e.g., filled thermoplastics), or a complex, multiphase fluid (e.g., the cement paste in fresh concrete). In general these may have dissolved ions and molecules that influence the interactions described above, via, e.g., a change of pH or dielectric constant. Here, we focus on Newtonian suspending fluids with constant viscosity η_f (see the sidebar titled Basic Rheological Quantities) and density ρ_f. The fluid contributes a dissipative stress scale $\eta_f\dot{\gamma}$ (for shear rate $\dot{\gamma}$) and ensures

BASIC RHEOLOGICAL QUANTITIES

- **Flow field:** The velocity field in the suspension $\boldsymbol{u}$. A uniform flow is one in which $\nabla\boldsymbol{u}$ is spatially invariant. For instance, a simple shear with rate $\dot{\gamma}$ such that $u_x = \dot{\gamma}y$ is uniform and has velocity gradient $(\nabla\boldsymbol{u})_{\alpha\beta} = \dot{\gamma}\delta_{\alpha x}\delta_{\beta y}$.
- **Strain rate:** The tensorial quantity $\mathcal{E}$ defined as the symmetric part of the velocity gradient: $\mathcal{E} \equiv (\nabla\boldsymbol{u} + \nabla\boldsymbol{u}^T)/2$. For a simple shear, $\mathcal{E}_{\alpha\beta} = \dot{\gamma}(\delta_{\alpha x}\delta_{\beta y} + \delta_{\alpha y}\delta_{\beta x})/2$.
- **Stress:** The tensorial quantity $\boldsymbol{\Sigma}$ describing the force per unit area acting on the suspension. We write a general shear stress as σ.
- **Viscosity:** The relation between $\mathcal{E}$ and the deviatoric part of $\boldsymbol{\Sigma}$. For a Newtonian fluid at pressure p, the viscosity η is a (single) scalar parameter, reflecting the material character: $\boldsymbol{\Sigma} = -p\boldsymbol{I} + 2\eta\mathcal{E}$.

incompressibility of the system, which plays a major role at macroscopic scales (e.g., 20). Additionally, thermal fluctuations in the fluid velocity generate Brownian forces on particles, which is especially relevant at the lower end of the particle-size range considered here (**Figure 2*g***).

2.3. Crowded Conditions

Although it has no formal definition, a dense suspension is usually taken to be one with solid and liquid mixed in roughly equal proportion. Under these conditions, the typical particle separation is smaller than the particle size, and small strains may bring their surfaces into contact (or near-contact). Short-range interactions such as pairwise repulsion/attraction are therefore important. Meanwhile, long-range, many-body hydrodynamics are screened by intervening particles, and the emerging consensus is that these are negligible in dense systems. Lubrication forces also remain relevant at a quantitative level only (21). With increasing ϕ, suspensions generically undergo a jamming transition, described later, from a flowable state to a solid state in which particle contact forces span the system. The exact nature of jamming is sensitive to particle-level details, but, as we discuss below, it bears some features of a continuous transition. Our focus is primarily on dense suspensions for which macroscopic behaviors are governed by physics associated with the proximity to this jamming transition.

2.4. Out of Equilibrium

For the particle-size range of interest here, Brownian motion, which is the restoring force toward equilibrium, may act over timescales comparable to, or longer than, a typical observation period. This can be quantified by the Stokes–Einstein relation for the diffusion coefficient $D \equiv k_B T/6\pi\eta_f a$ (with k_B the Boltzmann constant and T the temperature), leading to a diffusive timescale $a^2/D = 6\pi\eta_f a^3/k_B T$. For a small molecule this is $\approx 10^{-10}$ s, and the local state is always very near equilibrium. Meanwhile for a particle of radius $a = 1$ μm in water at room temperature it is ≈ 1 s. The a^3 dependence ensures that in many practical conditions, where typical timescales are indeed on the order of 1 s, Brownian forces can be neglected when $a > 1$ μm. Suspensions of such particles—these are called non-Brownian, athermal, or granular suspensions and are the focus of much of this article—are thus practically always out of equilibrium. The exploration of configuration space therefore occurs not by thermal motion but only as a result of external driving. Consequently there is strong history dependence, and statements about macroscopic phenomena must be associated with a characterization of the prior strain protocol. Without this, there is no reference (equilibrium-like) state.

This out-of-equilibrium nature leads to non-Newtonian macroscopic stresses. For simple fluids, which are Newtonian, normal and shear stresses are dominated by distinct physical mechanisms: The former come from the stiffness of molecular interactions; the latter come from molecular diffusion inducing momentum diffusion.

For suspensions, when describing the stress $\mathbf{\Sigma}$, one can distinguish the fluid stress $\mathbf{\Sigma}_f$ coming from the solvent (often a simple fluid for which the above considerations hold) from the particle stress $\mathbf{\Sigma}_p$ due to mechanical forces transmitted through the solid phase. With diffusion suppressed (or at least as slow as the shear itself), both normal and shear particle stresses originate in particles' inability to follow the fluid streamlines and their tendency to adopt a shear-induced structure (**Figure 2*b***). The particle (and, hence, the total) stress components are thus not independent of each other as they are for a simple liquid.

These distinguishing features make dense suspensions unamenable to an equilibrium description. We therefore proceed by first giving an overview of the out-of-equilibrium phase transitions necessary to understand their behavior.

3. OUT-OF-EQUILIBRIUM PHASE BEHAVIOR

Borrowing concepts from dry granular physics, we first address the phase transition of major relevance to much of the discussion that follows on non-Brownian suspensions jamming. We then give brief overviews of two transitions associated with Brownian suspensions (the glass transition) and suspensions of attractive particles, acknowledging that separate reviews should be consulted for these important topics (22, 23).

3.1. Jamming Transition

We consider non-Brownian, neutrally buoyant, repulsive particle suspensions, which generically transition from being flowable at low ϕ to being solid (and having a yield stress) at large ϕ. These limits are separated by a jamming transition, occurring at a critical volume fraction ϕ_J ($\approx$0.64 for monodisperse frictionless spheres) beyond which all motion is blocked due to widespread particle–particle contacts (as sketched in **Figure 2*e***). Above ϕ_J, a (quasi-static) strain can only occur by deforming the particles, which is not possible when they are rigid. Jamming is not specific to suspensions: It occurs in dry granular matter, emulsions, and other amorphous materials (24). It shares some features with equilibrium continuous phase transitions, especially diverging length scales, though other quantities, such as the number of contacts, may (depending upon the protocol; cf. the preparation dependence mentioned above) vary discontinuously across the transition (25).

The location of the transition, i.e., the value of ϕ_J, is sensitive to many microscopic details and also depends on the history of the sample (26). Most importantly, interparticle friction (quantified with dimensionless coefficients), which constrains rotational as well as translational particle motion, strongly affects jamming. All friction modes (sliding, rolling, and twisting) contribute to a decrease in ϕ_J (27), as does increasing the value of the friction coefficients. It is particle-shape (28, 29) and size-distribution dependent; broadening the particle-size distribution from monodisperse to polydisperse leads to a larger ϕ_J (30, 31).

These observations can be understood in a unified way by considering the appearance of isostaticity. The suspension jams when just enough particle contacts form to constrain all degrees of freedom in the system (32). This happens when the average number of contacts per particle z reaches a critical isostatic value z_c. In general, the value of z_c can be inferred from apparently simple Maxwellian constraint counting arguments (33), though this rapidly becomes involved for cases more complicated than frictionless spheres, as each contact may constrain multiple degrees of freedom (34). Below jamming, i.e., $\delta z \equiv z_c - z > 0$, the system is underconstrained, and there are $N\delta z/2$ floppy modes in a system of N particles. These modes represent collective degrees of freedom along which the system can be deformed without elastic cost. Floppy modes are spatially extended; due to the crowded conditions, moving a particle requires cooperative motion of other particles in the vicinity.

Jamming has some features consistent with a continuous transition. Structural and mechanical properties behave singularly as a function of the distance to jamming $\delta\phi \equiv \phi_J - \phi$ (or equivalently as a function of δz), and the associated exponents are often nontrivial (35, 36). In particular, several length scales diverge at the transition. Their identification and role are slowly emerging, with frictionless systems being better understood. The most relevant for this review is the correlation length of the velocity field (37) (or the nonaffine velocity field in the case of a sheared system), quantifying the cooperativity of motion in crowded conditions. Velocity correlations decay to zero on a typical length scale $l \sim \delta\phi^{-\lambda}$, with numerical results for frictionless spheres giving $\lambda \approx 0.6$–1 (38). They can be quantitatively linked to the statistics of floppy modes, and scaling theory predicts that $l \sim 1/\sqrt{\delta z}$ and $\lambda \approx 0.43$ (36).

This diverging length scale is central to the rheology close to jamming and is argued to be the origin of a divergence in the suspension viscosity η, occurring at ϕ_J (38). The physical picture is that correlated motion leads to nonaffine velocities via a lever effect, which results in enhanced viscous dissipation (39). The exact scaling relation (if any) between l and η is obscure, however, even for frictionless spheres. In a caricature of correlated motion in which particles are grouped in clusters of size l rotating as rigid bodies (40), equating for a cluster the injected power $\propto \eta\dot{\gamma}^2 l^d$ to the dissipated power $\propto n\eta_f\dot{\gamma}^2 a l^{d+2}$ (with n the particle number density), one finds that $\eta \propto l^2$. This is certainly too simplistic, however, as reaching ϕ_J from below the zero-shear viscosity (i.e., measured with infinitesimal shear stress) indeed diverges as $\eta \sim (\phi_J - \phi)^{-\beta}$, but with β being significantly larger than 2λ, as we show in Section 4. Indeed, though eddies following approximately a rigid-body motion have a size on the order of l and lead to the dominant decay of velocity correlations, there may be a secondary decay on a much longer length scale due to flow-induced contact anisotropy (41). The associated correlation length, diverging faster than l at jamming, would account for the viscosity divergence. The jamming transition is thus key to understanding the rheology of dense suspensions and forms a central part of our discussion in what follows, but it is not the only relevant transition.

3.2. Glass Transition

Brownian systems similarly undergo a transition from a flowable to a nonflowable state when ϕ increases. This is the colloidal glass transition, occurring at ϕ_G (42), above which particles are trapped in cages formed by their neighbors. The glass transition is distinct from jamming (43), and we refer to other reviews for details about its phenomenology (44). The most relevant aspects for Brownian suspensions in this review are that (*a*) the transition occurs before frictionless jamming, $\phi_G < \phi_J$ (for low polydispersity rigid spheres $\phi_G \approx 0.58$), (*b*) below ϕ_G the zero-shear viscosity diverges in a superexponential fashion, typically fitted with $\eta \sim \exp\{A/(\phi_G - \phi)^\delta\}$ (to be contrasted with the algebraic divergence at jamming), and (*c*) at ϕ_G a finite yield stress proportional to $k_B T$ (43) appears discontinuously (whereas at jamming the yield stress appears continuously).

3.3. A Note About Attractive Interactions

In the presence of attractive interactions, particles can stick together in clusters that eventually span the system, forming an elastic network with a yield stress (45). For Brownian systems, competition between $k_B T$ and attraction leads to complex ϕ dependence (46). The resulting colloidal glass and gelation behavior is an extensive and challenging topic and is reviewed elsewhere (see, e.g., 23). Meanwhile in non-Brownian systems the role of attraction near jamming is still emerging (47).

In what follows, we replace our labels for ϕ_J and ϕ_G with a more general, stress-dependent limiting volume fraction $\phi_m(\sigma)$, representing the value of ϕ at which the suspension viscosity η diverges. This is often still a jamming point, but in the presence of Brownian or attractive forces the divergence may have contributions from multiple phase transitions.

4. RHEOLOGY AND MICROSCOPIC PHYSICS

Having introduced the transitions that occur as ϕ approaches ϕ_m, we now discuss how the proximity to them is relevant in determining the macroscopic response, in particular the rheology under uniform flow (conditions in which the strain rate is spatially uniform). In general, the suspension viscosity η diverges at $\phi = \phi_m$, and complex rheology can be understood as stress- or

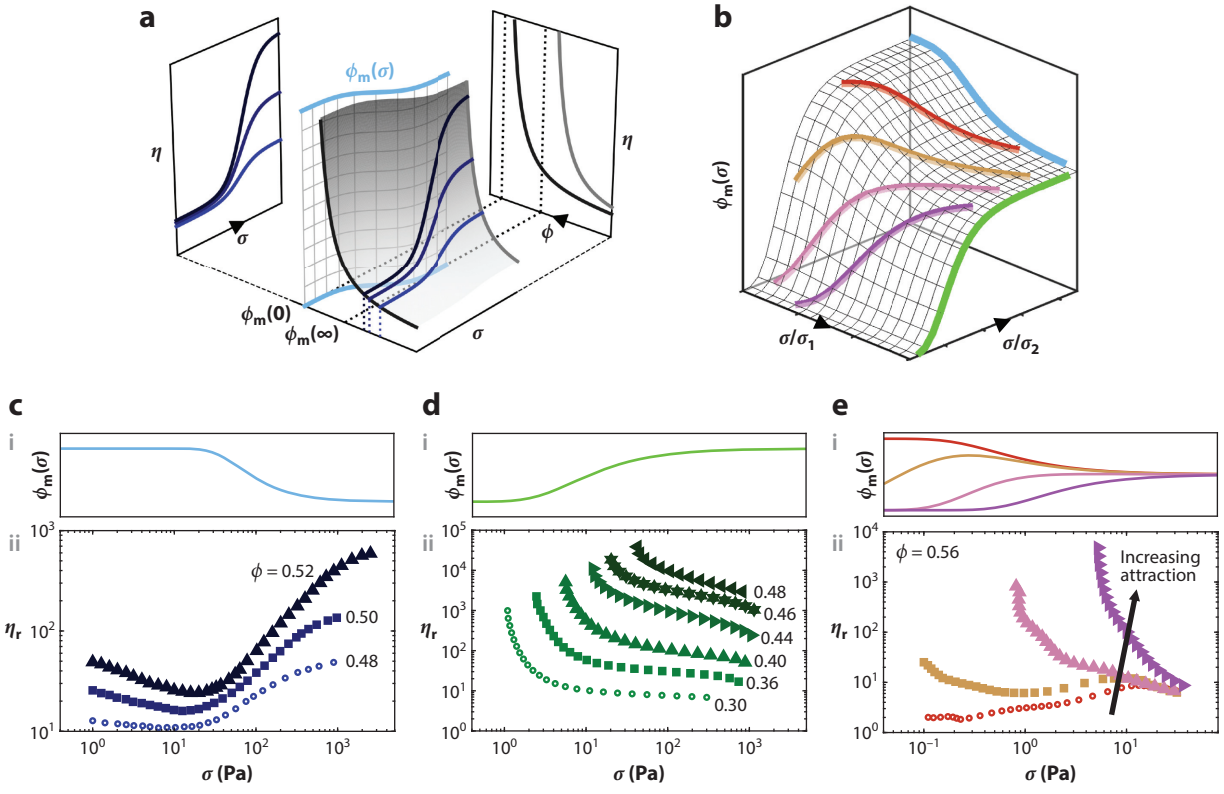

Figure 3

Dense suspension rheology, showing schematics (*a*, *b*, and *upper panels* of *c*, *d*, and *e*) and experimental data (*lower panels* of *c*, *d*, and *e*, with $\eta_r \equiv \eta/\eta_f$). (*a*) Schematic relating the viscosity $\eta(\sigma, \phi)$ to $\phi_m(\sigma)$. (*b*) Schematic showing qualitative $\phi_m(\sigma)$ behavior in the presence of one (*blue* and *green*) and two (*red* to *magenta*) characteristic stress scales, σ_1 and σ_2. (*c*, *i*) Schematic showing decreasing $\phi_m(\sigma)$; (*c*, *ii*) experimental data showing shear thickening in a suspension of $a \approx 260$ nm silica particles in a polyethylene glycol solvent at three different ϕ. (*d*, *i*) Schematic showing increasing $\phi_m(\sigma)$; (*d*, *ii*) experimental data showing shear thinning in a suspension of $a \approx 4$ μm ground calcium carbonate particles in a glycerol–water mixture at a range of ϕ. (*e*, *i*) Schematic showing $\phi_m(\sigma)$ for (*top* to *bottom*) increasing attraction; (*e*, *ii*) experimental data for a suspension of $a \approx 90$ μm soda-lime glass spheres in mineral oil at $\phi = 0.56$. Shown (*bottom* to *top*) are increasing applied electric field strengths, controlling attractive interactions. Panel *c* adapted with permission from Reference 61; copyright 2014 The Society of Rheology. Panel *d* adapted with permission from Reference 62; copyright 2021 Rheologica Acta. Panel *e* adapted with permission from Reference 63; copyright 2010 Springer Nature.

rate-controlled changes to the dominant microphysics, in many circumstances leading to stress dependence in ϕ_m itself. Such a scheme is sketched in **Figure 3*a***. Here, we illustrate how a monotonic $\phi_m(\sigma)$ (the physics of which we consider below) leads naturally to distinct stress-dependent viscosity divergences (whose form may follow, e.g., $\eta \sim [\phi_m(\sigma) - \phi]^{-\beta}$) and thus to rate-dependent rheology $\eta(\sigma, \phi)$. Rather than following a top-down approach to addressing macroscopic phenomenology, we instead consider systematically the microscale physics sketched in **Figure 2**. Our focus is not on the origin of microscopic forces per se but rather on their effect on the rheology. For experimental and computational methodologies—rheometry—we refer the reader to other reviews (see, e.g., 48, 49). We take as our starting point the idealized case of rate-independent suspensions (for which ϕ_m is independent of σ) before addressing rheology that arises in more complex cases, systematically examining physics one dimensionless parameter away from the rate-independent case.

4.1. A Reference Point: Rate-Independent Suspensions

Consider a dense suspension of non-Brownian, neutrally buoyant, rigid particles in a Newtonian fluid, subject to a steady deformation slow enough that fluid and particle inertia can be neglected. In practice this can be approximated with a suspension of ≈10 μm glass particles in an appropriate solvent under typical rheometric conditions. Such a system plays a special model role that has proven to be hugely influential in understanding many other classes of suspensions, as we discuss below.

4.1.1. Dimensional analysis. The microscopic quantities involved in the problem are the typical particle size a and density ρ_p, and the fluid viscosity η_f and density ρ_f (with $\rho_p = \rho_f$). For rigid particles there is no microscopic energy or force scale. The macroscopic quantities are the control volume size L (this is taken to be sufficiently larger than a so that we consider bulk phenomena) and the solid fraction ϕ therein. Finally, the deformation is characterized by its rate, $\dot{\gamma}$, the applied stress, σ, and the time for which it was applied, t. (This notation is conventional for simple shear, but the following argument applies generally.) Dimensional analysis implies that there are four dimensionless numbers besides ϕ. Appropriate choices are the Stokes number, $\mathrm{St} \equiv \rho_p \dot{\gamma} a^2/\eta_f$, the Reynolds number, $\mathrm{Re} \equiv \rho_f \dot{\gamma} L^2/\eta_f$, the relative suspension viscosity, $\eta_r \equiv \eta/\eta_f = \sigma/\eta_f \dot{\gamma}$, and the strain, $\gamma = \dot{\gamma} t$.

As stated earlier, we take as our reference point suspensions for which particle and fluid inertia can be neglected, corresponding, respectively, to $\mathrm{St} = 0$ and $\mathrm{Re} = 0$. We then conclude that η_r must be a function of ϕ and γ only. This is a strong statement: It implies that the stress is linear in the deformation rate, as for a Newtonian fluid, and that the proportionality factor, the suspension viscosity η, only depends on ϕ and γ. Furthermore, in steady state [the $\gamma \to \infty$ limit, in practice typically achieved for $\gamma = \mathcal{O}(1)$], η_r is a function of ϕ only.

This analysis (which follows Krieger; 50) can be extended to any component of the stress tensor, though these do not each necessarily share the same parity with $\dot{\gamma}$. Although shear stresses (or more generally the dissipative part of the stress tensor; 51) are linear in $\dot{\gamma}$, normal stresses, which for a rate-independent suspension are always negative (pushing outward), are linear in $|\dot{\gamma}|$. Depending on the system, the list of dimensionless numbers is augmented, most notably by the particle friction coefficient(s). Recent measurements show that friction is indeed a generic feature of direct contacts among micrometer (and larger) sized particles (15, 16), though the nondimensionality of the coefficient ensures (assuming friction is Coulombic) that this alone does not introduce rate dependence. This quasi-Newtonian result forms the basis for our discussion of more complex, rate-dependent suspensions in what follows.

4.1.2. Rheology under steady flow. Under a steady imposed deformation rate tensor, rate-independent suspensions can thus be characterized by a set of material functions (51) all depending on ϕ only. As expected from the discussion in Section 3.1, these are all singular at jamming, typically behaving asymptotically as $(\phi_m - \phi)^{-\beta}$ (4).

Here, ϕ_m typically represents a frictional jamming point (but see Section 4.4 below). Many experiments (4, 52) as well as simulations of spherical particle suspensions (39, 53) are consistent with $\beta \approx 2$, although quite different values have also been reported, with a possible dependence on the sliding friction coefficient μ_p (54–56). In a simplified model of frictionless sphere flow, for which the exponent can be determined with higher precision thanks to efficient numerical methods and to scaling theory linking β to other independently measurable exponents, one finds $\beta \approx 2.8$ (57). For long rod-like particles, it has been experimentally measured as $\beta \approx 1$ (58).

This rheology can also be formulated from an alternative (but equivalent), particle-pressure-imposed perspective. Boyer et al. (4) demonstrated (and verified experimentally) that in simple

shear the stress anisotropy, or macroscopic friction coefficient, i.e., μ (which in simple shear is $\mu \equiv \sigma/P_p$, with P_p a measure of the particle pressure), and ϕ are functions of the so-called viscous number $J \equiv \eta_f \dot{\gamma}/P_p$ only. Knowing $\mu(J)$ and $\phi(J)$, we can use the fact that $\eta/\eta_f = \mu(J)/J$ and invert the $\phi(J)$ relation to recover the volume-imposed rheology, that is, a rate-independent viscosity depending on ϕ only. Here, jamming corresponds to $J \to 0$. In this limit, $\phi(J) \sim \phi_m - aJ^{1/\beta}$ and $\mu(J) \sim \mu^* + bJ^{\xi}$ (4), such that $\eta \sim (\phi_m - \phi)^{-\beta}$. Importantly, μ^* is finite, implying that particle normal and shear stresses share the same asymptotics close to jamming. As with ϕ_m, μ^* depends on microscopic details. For frictionless ($\mu_p = 0$) spheres, $\mu^* \approx 0.1$ (59), whereas for $\mu_p \gtrsim 0.1$, $\mu^* \approx 0.3$–0.4 (60). Interestingly, the large friction limits for μ^* and ϕ_m occur at quite distinct values of μ_p (60).

4.1.3. Microstructure evolution and flow history dependence. For rate-independent suspensions, statements about the macroscopic rheology must be associated with a description of their strain history (though the rate at which this history was explored is unimportant). An initial transient of a few strain units [$\gamma = \mathcal{O}(1)$; 64] is generally observed upon flow start-up, after which the memory of initial conditions is lost and particles have, thanks to shear-induced diffusion (65), sampled a statistically representative part of the configuration space. Steady states (with $\gamma \gg 1$) are thus unambiguously defined, independent of the prior sample history, and are the usual reference points for characterizing rate-independent rheology.

Dense suspensions usually exhibit microstructural anisotropy, details of which depend on the deformation being applied (see, e.g., **Figure 2*b***). This is often characterized at the level of the statistics of some particle interaction director $\boldsymbol{n}$, usually via its averaged second moment, referred to as the structure, texture, or fabric tensor $\langle \boldsymbol{nn} \rangle$ (see also Section 5). During steady state flow, this tensor is often found to be aligned with the deformation rate tensor (66, 67). The microstructural anisotropy is mirrored at the macroscopic level by the stress anisotropy μ, although their exact relation remains elusive. For frictionless spheres near jamming, microstructural anisotropies bias the floppy mode statistics in favor of flow-resisting modes, leading to larger μ (36). Meanwhile, first and second normal stress differences quantify, respectively, stress anisotropy in and out of the flow plane (51, 54, 68).

Together, the finite transient in the strain (64, 69) and the shear-induced structure give rise to an anisotropic stress response: The viscosity of a rate-independent suspension is largest when the strain rate and microstructure tensors align. This is readily illustrated under unsteady flow conditions such as shear reversal (64) and oscillatory shear (70). When the direction of the applied flow changes more rapidly than a steady microstructure can establish (i.e., accumulating strains $\gamma < 1$ before reversal), the result is a systematically lower viscosity than in steady shear. An extreme case of this is the remarkable phenomenon of shear jamming (13, 71), in which a suspension is jammed under a previously applied deformation, but not jammed with respect to others. Separately, the behavior under repeated reversals reveals, for sufficiently small strain amplitude, contact-free states (72), indicating the presence of a nearby absorbing state (73).

4.2. Particle Inertia

At the upper end of our size range ($a \approx 1$ mm), particle inertia can be significant, i.e., $\mathrm{St} = \mathcal{O}(1)$, even at modest $\dot{\gamma}$. Dimensional analysis then implies an inertial stress that scales with $\rho_p a^2 \dot{\gamma}^2 g(\phi)$, the so-called Bagnold scaling (74), which is consistent with experimental (75, 76) and numerical (77–79) observation. Assuming that viscous ($\propto \dot{\gamma}$) and inertial ($\propto \dot{\gamma}^2$) stresses are additive, one concludes that the former will dominate at low shear rates and the latter at high rates, with a crossover occurring at $\dot{\gamma}_{in}$. Above $\dot{\gamma}_{in}$, the rate-independence described above thus gives way to a stress that is quadratic in $\dot{\gamma}$ (leading to $\eta \propto \dot{\gamma}$), which is a form of continuous shear thickening.

As with rate-independent flow, inertial rheology can be expressed in constant pressure terms. Whereas J characterizes the rheology under purely viscous conditions, the appropriate dimensionless shear rate under purely inertial conditions is the inertial number $I \equiv a\dot{\gamma}\sqrt{\rho_p/P_p}$ with μ and ϕ now functions of I only (80, 81). Generally, a viscous regime is expected for $\mathrm{St} = I^2/J \ll 1$, and an inertial one is expected for $\mathrm{St} \gg 1$ (79).

A central and unresolved question is that of the dependence (if any) of $\dot{\gamma}_{in}$ on ϕ when approaching ϕ_m. The inertial and viscous stresses are expected to scale, respectively, as $\dot{\gamma}^2(\phi_m - \phi)^{-\beta_i}$ and $\dot{\gamma}(\phi_m - \phi)^{-\beta_v}$ (81), with ϕ_m usually considered the same for both because inertia should not affect the isostaticity condition (though a stringent test of this is absent). Equating the stress contributions at the crossover leads to $\dot{\gamma}_{in} \sim (\phi_m - \phi)^{-\beta_v+\beta_i}$. Several numerical works report $\beta_v = \beta_i = 2$, or equivalently that μ and ϕ are functions of a composite number $K = J + \alpha I^2$ with $\phi_m - \phi \sim K^{1/2}$ (53, 79). Meanwhile others (82–84), as well as experiments (85), report $\beta_i > \beta_v$ (usually $\beta_i \approx 2\beta_v \approx 4$–5, which is compatible with scaling theory for flow near jamming (36, 56), which predicts $\beta_i = 2\beta_v \approx 5.7$), implying that inertia is relevant down to a Stokes number vanishing with proximity to jamming. However, the stress below which inertia can be neglected is $\eta\dot{\gamma}_{in} \sim (\phi_m - \phi)^{-2\beta_v+\beta_i}$, which remains finite at jamming if $\beta_i = 2\beta_v$.

4.3. Brownian Motion

Following the rule of thumb in Section 1, Brownian forces become important for particles with $a < 1$ μm, leading to the characteristic stress scale k_BT/a^3 (86) becoming relevant. Thermal fluctuations allow such Brownian particles to explore configuration space in the absence of external driving, so that an underlying equilibrium phase diagram might be defined (42) (though often in practice the system will not reach equilibrium over typical observable timescales).

Under flow, particle diffusion, which acts to redisperse any shear-induced microstructure and restore equilibrium, competes with convection, which drives the system out of equilibrium. The competition between the characteristic timescales for particle diffusion and convection is quantified by a dimensionless shear rate, the Péclet number $\mathrm{Pe} \equiv 6\pi\eta_f a^3\dot{\gamma}/k_BT$. This controls a crossover between the relative importance of the Brownian and viscous stresses. The former is sublinear in $\dot{\gamma}$ due to Pe dependence of the microstructure (87), and thus Brownian suspensions typically shear thin (88, 89). There may be a high shear (in practice this means $\mathrm{Pe} \gg 1$) viscosity plateau, where rate-independence is recovered (unless other physics intervenes; see below).

An alternative perspective may be to consider Brownian shear thinning as the consequence of a Pe-controlled change in the limiting volume fraction ϕ_m (43). It is established that the viscosities of Brownian and non-Brownian suspensions diverge at distinct points (5, 89), and these may be associated with the glass ϕ_G and jamming ϕ_J transitions, respectively (recalling that $\phi_J > \phi_G$). Hence, increasing Pe at a given ϕ leads to ϕ_m increasing from ϕ_G to ϕ_J, resulting in shear thinning (or indeed yielding if $\phi_G < \phi < \phi_J$; 43).

4.4. Repulsive Interactions

In reality, particles usually have repulsive interactions acting over a finite range, stabilizing them against clustering, inhibiting contact formation, and setting a force scale that is absent in the rigid particles considered so far. These interactions may originate in electrostatics, in polymer coatings, or from other physics (Brownian motion may provide an effective repulsion; 90). Importantly, a characteristic repulsive stress F_r/a^2 competes with the viscous one $\propto\eta_f\dot{\gamma}$, and a dimensionless shear rate can be defined, e.g., as $\dot{\gamma}/(F_r/\eta_f a^2)$. Details, including the range of the repulsive force, control how this quantity governs the effective proximity to ϕ_m and the consequent rate-dependence that emerges.

As mentioned in Section 4.1, direct contacts among micrometer (and larger) sized particles are typically frictional. The short-range repulsive interactions described above act to inhibit the formation of such contacts between particles, maintaining lubrication layers and, thus, limiting (in a stress-controlled manner) the role played by friction. The implications of this are profound and far-reaching (for a review, see Reference 7). As the applied stress σ is increased relative to an onset stress $\sigma^* \propto F_r/a^2$, the repulsive barrier is overcome and particle contacts increasingly transition from the lubricated to the frictional contact state. (The $1/a^2$ dependence ensures that particles larger than a few microns are persistently frictional.) With friction present, fewer contacts are required for mechanical equilibrium; i.e., z_c is reduced (34). ϕ_m will consequently reduce, from a frictionless limit $\phi_m^{(0)} \equiv \phi_m(\sigma/\sigma^* \to 0)$ to a lower, frictional value $\phi_m^{(1)} \equiv \phi_m(\sigma/\sigma^* \to \infty)$, as illustrated in **Figure 3**. Under fixed ϕ, therefore, increasing σ brings the suspension closer to jamming by reducing $\phi_m(\sigma) - \phi$. This frictional transition mechanism [encoded in a popular constitutive model (91) described later] provides a generic route to shear thickening that is distinct from the inertial Bagnoldian rheology described above (92). (When present, inertia may nonetheless contribute to mediation of particle contacts, thereby playing a role in a dynamic transition mechanism and enabling repulsionless frictional shear thickening; 15, 83.) It was proposed based on theory and simulation (14, 40, 91) and has been confirmed by a series of experiments (see 15, 93, and 94, among many others). Example experimental flow curves $\eta(\sigma, \phi)$ are shown in **Figure 3*c*** (61).

The extent of shear thickening increases as ϕ approaches $\phi_m^{(1)}$. Close to this value, the viscosity increase becomes discontinuous (theory predicts that $\dot{\gamma}$ becomes nonmonotonic in σ), whereas above this value flow stops at stresses of order σ^*. Shear thickening by this mechanism bears some hallmarks of a phase transition: increasing correlation lengths, stress fluctuations (95), and separation into lubricated and frictional states (96–98).

The above discussion applies generally to repulsive particles, whereas increasing the range of repulsion can introduce a separate effect. There exists a characteristic particle separation h for which the repulsive force balances the typical viscous force $\propto \eta_f \dot{\gamma} a^2$. Here, $a_{eff} \equiv (a + h/2)$ acts as the effective radius of a larger, soft particle, leading to an effective $\phi_{eff} > \phi$. The viscosity, now set by, e.g., $\eta \sim (\phi_m - \phi_{eff})^{-\beta}$, is thus enhanced by the presence of the repulsive force (there may even be a finite yield stress if $\phi_{eff} > \phi_m$). As $\dot{\gamma}$ increases, the force balance (assuming the repulsive force increases with decreasing separation) dictates that h decreases, as do a_{eff} and ϕ_{eff} (though this must remain $\geq \phi$). The system consequently moves further from ϕ_m, leading to reduced η. Low-$\dot{\gamma}$ shear thinning arising by this simple argument is a common feature of experimental rheology data (99).

4.5. Attractive Interactions

When present and sufficiently large, van der Waals (or other, for instance, depletion) forces lead to attraction between particles. This introduces a competition between aggregation processes (sticking particles together and providing elasticity; 100) and shearing processes (breaking particles apart). Steady shear generically breaks attractive bonds between particles, destroying larger flocs or clusters and leading to shear thinning (101–103), which is a typical characteristic of pastes (104). For Brownian particles, aggregation processes are well understood in the context of colloidal gelation (23), and their influence on the rheology is well established (5).

For non-Brownian particles, however, aggregation is instead driven by external forces, often shear itself (105). There is some evidence that the same general picture of shear thinning due to breaking aggregates applies both for weakly attractive particles (106) and rods (107), and for more strongly attractive systems (108, 109). In the absence of shear, meanwhile, numerical evidence (47) suggests that attraction reduces ϕ_m in non-Brownian, frictionless systems. Recent experimental measurements support the fact that weak attraction can enhance particle contacts (110) and even

stabilize them against rolling (62). The combination of attraction and restricted tangential motion, adhesion (or cohesion if the particles are identical), generates a yield stress at even lower volume fractions, details of which are heavily protocol dependent (111). Shearing at sufficiently large σ is argued to break adhesive contacts and relieve tangential constraints on particles; this is contrary to stress-induced friction, which introduces sliding constraints as the stress is increased. Under steady shear, therefore, ϕ_m is reported to increase with σ (see **Figure 3**), providing evidence that the yielding and shear-thinning rheology of attractive, non-Brownian suspensions [an example experimental flow curve $\eta(\sigma, \phi)$ is shown in **Figure 3*d***; 62] might be characterized within the same framework of stress-controlled changes to ϕ_m (112; see also 113). It is not yet clear whether the few numerical works on attractive, frictional suspensions corroborate this (114, 115), in part due to the challenge of precisely defining particle contact models comprising attraction, rolling, and sliding friction.

4.6. More Complex Suspensions

Most suspensions will, in practice, have more than one relevant stress scale, with various physics from the sections above being important under typical operating conditions. For example, the combined effects of increasing and decreasing ϕ_m due to, respectively, an adhesive stress (62) (or indeed a Brownian stress; 116) and a repulsive stress can lead to nonmonotonic rheology. We show such an example in **Figure 3*e***, taking experimental data from Reference 63 (another example is Reference 117). By tuning the relative importance of one of the dimensionless groups (in the example shown, this is achieved by manipulating the attraction), one tunes between shear thinning and thickening rheology. This might be characterized as a transition, as a function of σ, across a multidimensional ϕ_m map (**Figure 3*b***). Here, we plot such a surface (following Reference 112; see Section 5.2) comprising both ϕ_m-reducing and ϕ_m-increasing physics. Besides the limiting cases depending on only one stress scale (**Figure 3*b*** shows both a typical shear-thickening suspension and an adhesive, shear-thinning one), a more general scenario with two (or more) stress scales ($\sigma_1, \sigma_2, \ldots$) that lead to much richer $\phi_m(\sigma)$ may be useful to interpret the rheology of more complex suspensions. For instance, **Figure 3*e*** links complex experimental rheological data to the putative $\phi_m(\sigma)$ map sketched in **Figure 3*b***. It is, however, still too early to assert this scenario, and more experimental, numerical, and theoretical work in this direction is needed.

Dense suspensions with a broad particle-size distribution present more complexity still. Although polydispersity is known to increase ϕ_m and consequently decrease the viscosity of rate-independent suspensions (30), the effect of broad polydispersity on rate-dependent rheology is not well understood. Whereas for roughly monodisperse suspensions the microscopic stress scales described above map to macroscopic ones, for polydisperse suspensions this is more involved. In practice, particle radii a may span six orders of magnitude (104). In such cases it is not clear how to define bulk dimensionless control parameters, which have, for instance, $\mathrm{St} \propto a^2$, $\mathrm{Pe} \propto a^3$, and contact friction onset $\sigma^* \propto 1/a^2$. Extending the descriptions above to such systems poses a challenge (118), as do numerous other sources of complexity (we list a few as Future Issues below).

5. CONTINUUM MODELS AND FLUID MECHANICS

The above insights can be utilized to make predictions of suspension behavior in practical scenarios. Doing so requires continuum models, giving the time evolution of the velocity field, which is driven by the stress field through the Cauchy equation, and other macroscopically relevant fields (the list of which is itself a modeling challenge), such as microstructure and volume fraction. Such models must combine conservation laws with closures for the coupling terms relating the different fields.

We first address constitutive equations, i.e., closures relating the stress tensor to the (history of) deformation. These should describe both steady and transient phenomena, the latter encoding the relative slowness (dictated by the shear rate) of the microstructural evolution. We limit the discussion to local models, acknowledging that nonlocal phenomena, relatively well studied in dry granular matter (see, e.g., 119, 120), likely play a role in suspensions near ϕ_m. We then give a brief introduction to two-phase continuum equations, which is necessary for describing flows involving migration, i.e., relative motion between solid and liquid phases (**Figure 2*i***). We conclude with a brief overview of some relevant aspects of the fluid mechanics of dense suspensions.

5.1. Rate-Independent Microstructural Constitutive Models

As briefly introduced in Section 4.1, the stress is strongly coupled to the anisotropy of the microstructure. The mathematical nature of the stress (being a second-order, symmetric tensor) naturally calls for a coupling with a suitably defined fabric tensor. The main approach for rate-independent suspensions thus follows the anisotropic fluid theory of Hand (121). This addresses the time evolution of a fabric tensor $\langle \boldsymbol{nn} \rangle$ under a velocity gradient tensor $\nabla \boldsymbol{u}$. The director $\boldsymbol{n}$ represents, for instance, the orientation of particle contacts, and the components of the fabric tensor are $\langle \boldsymbol{nn} \rangle_{\alpha\beta} = \langle n_\alpha n_\beta \rangle$. If $\boldsymbol{n}$ is not uniformly distributed, its typical orientation is given by the eigenvector of $\langle \boldsymbol{nn} \rangle$ associated to the largest eigenvalue. Such a theory then consists of an expression for the stress tensor $\boldsymbol{\Sigma}$ as a function of $\langle \boldsymbol{nn} \rangle$ and the symmetric part of the deformation rate tensor $\mathcal{E} \equiv (\nabla \boldsymbol{u} + \nabla \boldsymbol{u}^T)/2$, and a dynamics for $\langle \boldsymbol{nn} \rangle$. The latter depends on $\nabla \boldsymbol{u}$ and is constrained by frame indifference when particle inertia is negligible (see section 4.3 in Reference 122), and for a homogeneous system is:

$$\boldsymbol{\Sigma} = \boldsymbol{\Sigma}(\langle \boldsymbol{nn} \rangle, \mathcal{E}), \qquad \frac{\mathrm{D}\langle \boldsymbol{nn} \rangle}{\mathrm{D}t} = \mathcal{F}(\langle \boldsymbol{nn} \rangle, \mathcal{E}), \tag{1.}$$

with $\mathrm{D}\langle \boldsymbol{nn} \rangle/\mathrm{D}t \equiv \mathrm{d}\langle \boldsymbol{nn} \rangle/\mathrm{d}t + \langle \boldsymbol{nn} \rangle \cdot \boldsymbol{\Omega} - \boldsymbol{\Omega} \cdot \langle \boldsymbol{nn} \rangle$ the corotational (or Jaumann) derivative and $\boldsymbol{\Omega} \equiv (\nabla \boldsymbol{u} - \nabla \boldsymbol{u}^T)/2$. There are two routes to such a theory. The first is a phenomenological one, in which one keeps the structural form of these equations as general as permitted by symmetries (e.g., 123–125), which keeps the theory flexible at the cost of having many free parameters and little understanding of their microscopic origin. The other route is microstructural, with $\mathcal{F}(\langle \boldsymbol{nn} \rangle, \nabla \boldsymbol{u})$ derived from particle dynamics using simplifying assumptions (126–128). This limits the number of free parameters but involves (often uncontrolled) approximations, in particular the closure of higher moments of $\boldsymbol{n}$, such as $\langle \boldsymbol{nnnn} \rangle$ in terms of $\langle \boldsymbol{nn} \rangle$ (124, 129). Although phenomenological models can achieve quantitative agreement with experimental data regarding the transient behavior of the shear stress in simple shear (125), their predictions for normal stresses (when tested) are usually poorer (124, 130) (although some aspects of the steady state behavior can be captured; 131).

A recent work revisited the microstructural route based on the physical picture of a nearby jamming transition, giving a quantitative agreement with simulations for shear stresses and a qualitative one for normal stresses (128). The key assumption is that due to the one-sidedness of rigid particle contacts (which dominate the rheology close to jamming), the microstructure reacts in a strikingly different manner to compressive and extensional strains. This motivates a phenomenological theory in which, defining a decomposition $\mathcal{E} = \mathcal{E}_c + \mathcal{E}_e$, one gives distinct roles to the compressive $\mathcal{E}_c$ and extensional $\mathcal{E}_e$ strain rate tensors in the dynamics of $\langle \boldsymbol{nn} \rangle$ and in the stress–structure relation (132).

These rate-independent equations may constitute a basis for the development of constitutive models for suspensions with more complex interactions, as we discuss in the next subsection. It should however be noted that so far, even for works following the microstructural route, the

stress–structure relation is phenomenological and not derived from the microscopic dynamics. In particular, the viscosity divergence at jamming, when considered, is assumed to follow the algebraic form discussed in Section 4. Microscopically derived tensorial stress–structure relations are still lacking, even though real progress has been achieved for scalar relations in model suspensions (36, 56).

5.2. Constitutive Models for Rate-Dependent Suspensions

A typical approach in writing steady state rheological models is to define (for fixed ϕ) limiting $\eta_0 \equiv \eta(\dot{\gamma} \to 0)$ and $\eta_\infty \equiv \eta(\dot{\gamma} \to \infty)$ (in principle these can be measured experimentally) and then specify a smooth transition between them as a function of, e.g., $\dot{\gamma}_c/\dot{\gamma}$ or σ_c/σ (133). Such rheological interpolation models are widely used for the fitting of data (5), and in some instances $\dot{\gamma}_c$ (or σ_c) may provide microstructural insight (101).

As discussed in Section 4, the physics and rheology of several important classes of dense suspensions can be described as the result of an alteration of ϕ_m under flow due to the competition between applied stress and microscopic interparticle forces. This basic mechanism can be formalized with rheological interpolation models that do have a microscopic grounding, as shown initially by Wyart & Cates (91) in the context of shear thickening, and later extended by others (112).

These models address the activation and release, under stress, of particle-level constraints. These are pairwise interactions that reduce the number of degrees of freedom along which particle motion can occur (e.g., through friction or adhesion), thus altering ϕ_m. A measure of the degree of constraint is encoded in a fraction of activated constraints f, which is a function of some component of the applied stress, say, the shear stress σ (some models instead use the particle pressure; 91). This function is usually given a sigmoidal shape around the typical stress σ_c needed to switch a microscopic constraint, such that $f(\sigma \ll \sigma_c) \to 0$ and $f(\sigma \gg \sigma_c) \to 1$. In turn, ϕ_m depends on f. In the absence of the microscopic constraint (for instance, the absence of frictional contacts in the discussion in Section 4.4), $\phi_m(f = 0) = \phi_m^{(0)}$, whereas when the constraints are fully activated $\phi_m(f = 1) = \phi_m^{(1)}$ (for frictional contacts, $\phi_m^{(1)} < \phi_m^{(0)}$). As sketched in **Figure 3*a***, ϕ_m controls the viscosity through the divergence of η as, say, $\eta \sim (\phi_m - \phi)^{-2}$ (but this specific form is not a requirement). η is then an implicit function of σ, interpolating between $\eta = (\phi_m^{(0)} - \phi)^{-2}$ for $\sigma \ll \sigma_c$ and $\eta = (\phi_m^{(1)} - \phi)^{-2}$ for $\sigma \gg \sigma_c$. These models have been quite successful at predicting steady state rheology (93, 134) and also inhomogeneous flows and instabilities (69, 98; see also Reference 135 for an independent model with similar structure).

This mechanism can be extended to arbitrary numbers of constraint types and activation (or release) stresses, leading to a wide range of possible predicted rheologies (112; see examples in **Figure 3*b–e***). Such Wyart–Cates-like interpolation models can also be extended to tensorial constitutive laws (136, 137) and constant particle pressure rheology (91, 138). Although these models are motivated by a microscopic mechanism, they are in practice still phenomenological: In addition to the phenomenological viscosity divergence law, the relation $f(\sigma)$ is usually postulated, although it is suggested that it is controlled by force chain physics (92, 93, 134). This opens the possibility of deriving $f(\sigma)$ from microscopic statistical models (139).

5.3. Two-Phase Description

Many flows involve inhomogeneous deformation, sedimentation, or particle migration (**Figure 2*i***), and one cannot describe the suspension as a single-phase continuum. For these flows the composition of the suspension evolves continuously in space and time, making them amenable to a two-phase description in which particle and fluid phases are treated as interpenetrating continua comprising a volume fraction field and coupled velocity and stress fields for each phase. Such

a model consists of conservation laws written separately for the solid and fluid phases, which one can obtain via local volumetric averages (140). These involve a decomposition of the suspension stress into solid and fluid phase contributions (which are independently measurable; 141, 142), as well as a coupling term in the form of an interphase drag.

However, these equations do not form a closed system, as the stresses and interphase drag have no exact expression in terms of phase velocities or volume fraction. Stresses are closed with a constitutive model, as discussed in the previous subsections. A popular drag closure is the suspension balance model (143, 144), which consists of expressing the drag term as proportional to the relative velocity between the two phases. This is in essence closely related to the approximation behind Darcy's law for fluid flow through a porous solid phase. These aspects and their implications are addressed in a recent review (6).

5.4. Fluid Mechanics

Most flows of dense suspensions—especially in nature and in engineering—are not well-approximated by spatially homogeneous, rheometric conditions. Instead, they typically involve spatial and temporal inhomogeneities in the stress, strain rate, and volume fraction. These situations are currently the focus of a significant research effort, drawing attention to several subtle aspects introduced below.

The bulk effective fluid description of dense suspensions presented in the previous sections is certainly a key tool to understanding fluid mechanical phenomena, but it is not sufficient in itself. Flows involving nonuniform conditions require a two-phase description as described above, and raise the question of the nonlocality of constitutive models (145). Nonuniform systems can also be the result of instabilities, due to underlying nonmonotonic flow curves, leading to banding (146) or dynamic instabilities (20, 95, 98, 135, 147–149). Shear-induced migration is also important in nonuniform conditions (7, 150–152). Remarkably, there is a growing body of evidence that these instabilities are coupled to macroscopic deformation of the free surface, when present (97, 148, 153, 154).

The free surface poses a challenge as it represents a deformable confinement, constrained by both capillary forces and the incompressibility of the solvent. This is in striking contrast to dry granular systems, which are free to dilate. The role of the free surface in the flow of dense suspensions is in general subtle, as the large particle size makes it easy for particles to individually deform the solvent–air interface. Curving a free surface on a particle-radius scale a requires a stress scaling as $1/a$ to counteract the effect of capillary forces (see **Figure 2*j***). For micron-sized particles, this is easily achieved even in a rheometer, and particle-poking through the interface or a visible mattification of the surface is often reported (9). The free surface is then a nontrivial boundary condition for the fluid mechanical problem, and in practice it is not well approximated by either constant volume or constant pressure conditions (155). The crucial role of the grain scale deformation of the free surface is highlighted by situations in which the interface slowly recedes, like unwetting or drying, which often leads to interface instabilities, particle deposition patterns, and granulation (156–159). All these phenomena call for a careful modeling of the suspension free surface at the microscale, which is little-explored thus far, at least in the context of dense suspension rheology.

6. CLOSING REMARKS

We have presented a perspective on the physics of dense suspensions. Interpreting the macroscopic phenomenology of real suspensions and constructing continuum descriptions on the basis of the simple microscopic arguments introduced here will clearly be nontrivial in most cases. Nonetheless, what we have presented are foundational concepts from which descriptions of more

complex systems can be assembled. Doing so will require further study in many areas, some of which we propose below as Future Issues. Given the ubiquity of dense suspensions as both a model system in condensed matter physics and an engineering material, there is no doubt that they will remain a topic of research and debate in the future.

FUTURE ISSUES

1. Can suspensions of nonidealized particles (aggregates, fibers, rods, with arbitrary polydispersity) be approached by analogy to nearly monodisperse spheres, that is, only adjusting the values of key parameters like ϕ_m and the exponent β?
2. How far can the insights presented here be carried to the physics of suspensions with non-Newtonian solvents? Recent work suggests that in some cases the rheology can be captured by an effective local shear rate in the solvent, controlled by geometry close to jamming (160).
3. The sensitivity of the jamming transition to the nature of particle contacts calls for more attention to, in particular, the physics of contacts with a few surface asperities (as opposed to the multicontact interface paradigm of friction between macroscopic particles; 19).
4. The statistical physics connecting microscopic details to flow close to jamming is limited to frictionless spheres (36, 41). Is the floppy mode paradigm relevant with friction present (56)?
5. Suspensions with nonrigid constraints often have elastic structures. Can viscous continuum models such as those described above be augmented to account for these?
6. The boundary condition provided by free surfaces plays a major role but is poorly understood because it often involves particle-size curvature. What aspects of interfacial physics (such as contact angle and roughness anchoring) matter most at the boundary?
7. More generally, to what extent do the simplifications made here (limited role of hydrodynamics, rheometric conditions, etc.) need to be relaxed in order to describe real flows, which may involve instabilities and secondary structures?

DISCLOSURE STATEMENT

The authors are not aware of any affiliations, memberships, funding, or financial holdings that might be perceived as affecting the objectivity of this review.

ACKNOWLEDGMENTS

The authors thank M. Cates and E. Guazzelli for commenting on the manuscript. C.N. acknowledges support from the Royal Academy of Engineering under the Research Fellowship scheme. The work was supported by the startup fund of Wenzhou Institute, University of Chinese Academy of Sciences (No. WIUCASQD2020002) and National Natural Science Foundation of China (No. 1217042129).

LITERATURE CITED

1. Einstein A. 1911. *Ann. Phys.* 339(3):591–92
2. Batchelor GK. 1970. *J. Fluid Mech.* 41(3):545–70

3. Fuchs M, Cates ME. 2002. *Phys. Rev. Lett.* 89(24):248304
4. Boyer F, Guazzelli É, Pouliquen O. 2011. *Phys. Rev. Lett.* 107(18):188301
5. Mewis J, Wagner NJ. 2012. *Colloidal Suspension Rheology*. Cambridge, UK: Cambridge Univ. Press
6. Guazzelli É, Pouliquen O. 2018. *J. Fluid Mech.* 852:P1
7. Morris JF. 2020. *Annu. Rev. Fluid Mech.* 52:121–44
8. Denn MM, Morris JF. 2014. *Annu. Rev. Chem. Biomol. Eng.* 5(1):203–28
9. Zhou J, Dupuy B, Bertozzi AL, Hosoi AE. 2005. *Phys. Rev. Lett.* 94(11):117803. **https://doi.org/10.1103/PhysRevLett.94.117803**
10. Fusier J, Goyon J, Chateau X, Toussaint F. 2018. *J. Rheol.* 62(3):753–71
11. Bossis G, Boustingorry P, Grasselli Y, Meunier A, Morini R, et al. 2017. *Rheol. Acta* 56(5):415–30
12. Israelachvili JN. 2011. *Intermolecular and Surface Forces*. New York: Academic
13. Cates ME, Wittmer JP, Bouchaud JP, Claudin P. 1998. *Phys. Rev. Lett.* 81:1841–44
14. Seto R, Mari R, Morris JF, Denn MM. 2013. *Phys. Rev. Lett.* 111(21):218301
15. Fernandez N, Mani R, Rinaldi D, Kadau D, Mosquet M, et al. 2013. *Phys. Rev. Lett.* 111(10):108301
16. Comtet J, Chatté G, Niguès A, Bocquet L, Siria A, Colin A. 2017. *Nat. Commun.* 8:15633
17. Johnson KL. 1985. *Contact Mechanics*. Cambridge/New York: Cambridge Univ. Press
18. Chatté G, Comtet J, Niguès A, Bocquet L, Siria A, et al. 2018. *Soft Matter* 14(6):879–93
19. Lobry L, Lemaire E, Blanc F, Gallier S, Peters F. 2019. *J. Fluid Mech.* 860:682–710
20. Nagahiro Si, Nakanishi H. 2016. *Phys. Rev. E* 94:062614
21. Maiti M, Heussinger C. 2014. *Phys. Rev. E* 89(5):052308
22. Berthier L, Biroli G. 2011. *Rev. Mod. Phys.* 83(2):587–645
23. Zaccarelli E. 2007. *J. Phys. Condens. Matter* 19(32):323101
24. Liu AJ, Nagel SR. 1998. *Nature* 396(6706):21–22
25. Liu AJ, Nagel SR. 2010. *Annu. Rev. Condens. Matter Phys.* 1:347–69
26. Torquato S, Truskett TM, Debenedetti PG. 2000. *Phys. Rev. Lett.* 84(10):2064–67
27. Santos AP, Bolintineanu DS, Grest GS, Lechman JB, Plimpton SJ, et al. 2020. *Phys. Rev. E* 102(3):032903
28. Donev A, Cisse I, Sachs D, Variano EA, Stillinger FH, et al. 2004. *Science* 303(5660):990–93
29. Hsiao LC, Jamali S, Glynos E, Green PF, Larson RG, Solomon MJ. 2017. *Phys. Rev. Lett.* 119(15):158001
30. Shapiro AP, Probstein RF. 1992. *Phys. Rev. Lett.* 68(9):1422–25
31. Hopkins AB, Stillinger FH, Torquato S. 2013. *Phys. Rev. E* 88(2):022205
32. Alexander S. 1998. *Phys. Rep.* 296(2–4):65–236
33. Maxwell JC. 1864. *Lond. Edinb. Dublin Philos. Mag. J. Sci.* 27(182):294–99
34. Shundyak K, van Hecke M, van Saarloos W. 2007. *Phys. Rev. E* 75(1):010301
35. Liu AJ, Nagel SR, van Saarloos W, Wyart M. 2011. In *Dynamical Heterogeneities in Glasses, Colloids, and Granular Media*, ed. L Berthier, G Biroli, J-P Bouchaud, L Cipeletti, W van Saarloos, pp. 298–340. Oxford/New York: Oxford Univ. Press
36. DeGiuli E, Düring G, Lerner E, Wyart M. 2015. *Phys. Rev. E* 91(6):062206
37. Olsson P, Teitel S. 2007. *Phys. Rev. Lett.* 99(17):178001
38. Heussinger C, Barrat JL. 2009. *Phys. Rev. Lett.* 102(21):218303
39. Andreotti B, Barrat JL, Heussinger C. 2012. *Phys. Rev. Lett.* 109(10):105901
40. Heussinger C. 2013. *Phys. Rev. E* 88(5):050201
41. Düring G, Lerner E, Wyart M. 2014. *Phys. Rev. E* 89(2):022305
42. Pusey PN, Van Megen W. 1986. *Nature* 320(6060):340–42
43. Ikeda A, Berthier L, Sollich P. 2012. *Phys. Rev. Lett.* 109(1):018301
44. Hunter GL, Weeks ER. 2012. *Rep. Prog. Phys.* 75(6):066501
45. Trappe V, Prasad V, Cipelletti L, Segre PN, Weitz DA. 2001. *Nature* 411(6839):772–75
46. Larson RG. 1999. *The Structure and Rheology of Complex Fluids*. New York/Oxford: Oxford Univ. Press
47. Koeze DJ, Tighe BP. 2018. *Phys. Rev. Lett.* 121(18):188002
48. Coussot P. 2016. *Rheophysics: Matter in All Its States*. Cham, Switz.: Springer
49. Maxey M. 2017. *Annu. Rev. Fluid Mech.* 49:171–93
50. Krieger IM. 1963. *Trans. Soc. Rheol.* 7(1):101–9
51. Giusteri GG, Seto R. 2018. *J. Rheol.* 62(3):713–23

52. Ovarlez G, Bertrand F, Rodts S. 2006. *J. Rheol.* 50(3):259–92
53. Ness C, Sun J. 2015. *Phys. Rev. E* 91(1):012201
54. Zarraga IE, Hill DA, Leighton DT. 2000. *J. Rheol.* 44(2):185–220
55. Gallier S, Lemaire E, Lobry L, Peters F. 2014. *J. Comput. Phys.* 256:367–87
56. Trulsson M, DeGiuli E, Wyart M. 2017. *Phys. Rev. E* 95(1):012605
57. Lerner E, Düring G, Wyart M. 2012. *PNAS* 109(13):4798–803
58. Tapia F, Shaikh S, Butler JE, Pouliquen O, Guazzelli E. 2017. *J. Fluid Mech.* 827:R5
59. da Cruz F, Emam S, Prochnow M, Roux J-N, Chevoir F. 2005. *Phys. Rev. E* 72(2):021309
60. Chèvremont W, Chareyre B, Bodiguel H. 2019. *Phys. Rev. Fluids* 4(6):064302
61. Cwalina CD, Wagner NJ. 2014. *J. Rheol.* 58(4):949–67
62. Richards JA, O'Neill RE, Poon WCK. 2021. *Rheol. Acta* 60:97–106
63. Brown E, Forman NA, Orellana CS, Zhang H, Maynor BW, et al. 2010. *Nat. Mater.* 9(3):220–24
64. Gadala-Maria F, Acrivos A. 1980. *J. Rheol.* 24(6):799–814
65. Leighton D, Acrivos A. 1987. *J. Fluid Mech.* 177:109–31
66. Parsi F, Gadala-Maria F. 1987. *J. Rheol.* 31(8):725–32
67. Brady JF, Morris JF. 1997. *J. Fluid Mech.* 348:103–39
68. Seto R, Giusteri GG. 2018. *J. Fluid Mech.* 857:200–15
69. Han E, Wyart M, Peters IR, Jaeger HM. 2018. *Phys. Rev. Fluids* 3(7):073301
70. Blanc F, Lemaire E, Peters F. 2014. *J. Fluid Mech.* 746:R4
71. Seto R, Singh A, Chakraborty B, Denn MM, Morris JF. 2019. *Granul. Matter* 21(3):82
72. Pine DJ, Gollub JP, Brady JF, Leshansky AM. 2005. *Nature* 438(7070):997–1000
73. Tjhung E, Berthier L. 2015. *Phys. Rev. Lett.* 114(14):148301
74. Bagnold RA. 1954. *Proc. R. Soc. Lond. Ser. A. Math. Phys. Sci.* 225(1160):49–63
75. Savage SB, Mckeown S. 1983. *J. Fluid Mech.* 127:453–72
76. Madraki Y, Oakley A, Nguyen Le A, Colin A, Ovarlez G, Hormozi S. 2020. *J. Rheol.* 64(2):227–38
77. Verberg R, Koch DL. 2006. *Phys. Fluids* 18(8):083303
78. Kulkarni PM, Morris JF. 2008. *Phys. Fluids* 20(4):040602
79. Trulsson M, Andreotti B, Claudin P. 2012. *Phys. Rev. Lett.* 109(11):118305
80. Jop P, Forterre Y, Pouliquen O. 2006. *Nature* 441(7094):727–30
81. Lemaître A, Roux JN, Chevoir F. 2009. *Rheol. Acta* 48(8):925–42
82. Otsuki M, Hayakawa H. 2009. *Prog. Theor. Phys.* 121(3):647–55
83. Otsuki M, Hayakawa H. 2011. *Phys. Rev. E* 83(5):051301
84. Vågberg D, Olsson P, Teitel S. 2016. *Phys. Rev. E* 93(5):052902
85. Fall A, Lemaitre A, Bertrand F, Bonn D, Ovarlez G. 2010. *Phys. Rev. Lett.* 105(26):268303
86. Batchelor GK. 1977. *J. Fluid Mech.* 83(1):97–117
87. Foss DR, Brady JF. 2000. *J. Fluid Mech.* 407:167–200
88. Woods ME, Krieger IM. 1970. *J. Colloid Interface Sci.* 34(1):91–99
89. de Kruif CG, van Iersel EMF, Vrij A, Russel WB. 1985. *J. Chem. Phys.* 83(9):4717–25
90. Trulsson M, Bouzid M, Kurchan J, Clément E, Claudin P, Andreotti B. 2015. *Europhys. Lett.* 111(1):18001
91. Wyart M, Cates M. 2014. *Phys. Rev. Lett.* 112(9):098302
92. Ness C, Sun J. 2016. *Soft Matter* 12(3):914–24
93. Guy BM, Hermes M, Poon WCK. 2015. *Phys. Rev. Lett.* 115(8):088304
94. Lin NY, Guy BM, Hermes M, Ness C, Sun J, et al. 2015. *Phys. Rev. Lett.* 115(22):228304
95. Rathee V, Blair DL, Urbach JS. 2017. *PNAS* 114(33):8740–45
96. Fall A, Bertrand F, Ovarlez G, Bonn D. 2009. *Phys. Rev. Lett.* 103(17):178301
97. Hermes M, Guy BM, Poon WC, Poy G, Cates ME, Wyart M. 2016. *J. Rheol.* 60(5):905–16
98. Chacko RN, Mari R, Cates ME, Fielding SM. 2018. *Phys. Rev. Lett.* 121(10):108003
99. Maranzano BJ, Wagner NJ. 2001. *J. Rheol.* 45(5):1205–22
100. Rueb C, Zukoski C. 1997. *J. Rheol.* 41(2):197–218
101. Cross MM. 1965. *J. Colloid Sci.* 20(5):417–37
102. Woutersen ATJM, de Kruif C. 1991. *J. Chem. Phys.* 94(8):5739–50
103. Rueb C, Zukoski C. 1998. *J. Rheol.* 42(6):1451–76

104. Roussel N, Lemaître A, Flatt RJ, Coussot P. 2010. *Cement Concrete Res.* 40(1):77–84
105. Guery J, Bertrand E, Rouzeau C, Levitz P, Weitz D, Bibette J. 2006. *Phys. Rev. Lett.* 96(19):198301
106. Snabre P, Mills P. 1996. *J. Phys. III* 6(12):1811–34
107. Chaouche M, Koch DL. 2001. *J. Rheol.* 45(2):369–82
108. Zhou JZ, Uhlherr PH, Luo FT. 1995. *Rheol. Acta* 34(6):544–61
109. Kurokawa A, Vidal V, Kurita K, Divoux T, Manneville S. 2015. *Soft Matter* 11(46):9026–37
110. Park N, Rathee V, Blair DL, Conrad JC. 2019. *Phys. Rev. Lett.* 122(22):228003
111. Richards JA, Guy BM, Blanco E, Hermes M, Poy G, Poon WCK. 2020. *J. Rheol.* 64(2):405–12
112. Guy BM, Richards JA, Hodgson DJM, Blanco E, Poon WCK. 2018. *Phys. Rev. Lett.* 121(12):128001
113. Wildemuth C, Williams M. 1984. *Rheol. Acta* 23(6):627–35
114. Pednekar S, Chun J, Morris JF. 2017. *Soft Matter* 13(9):1773–79
115. Singh A, Pednekar S, Chun J, Denn MM, Morris JF. 2019. *Phys. Rev. Lett.* 122(9):098004
116. Laun HM. 1984. *Die Angew. Makromol. Chem.: Appl. Macromol. Chem. Phys.* 123(1):335–59
117. Gopalakrishnan V, Zukoski C. 2004. *J. Rheol.* 48(6):1321–44
118. Guy BM, Ness C, Hermes M, Sawiak LJ, Sun J, Poon WCK. 2019. *Soft Matter* 16(1):229–37
119. Bouzid M, Izzet A, Trulsson M, Clément E, Claudin P, Andreotti B. 2015. *Eur. Phys. J. E* 38(11):125
120. Kamrin K, Koval G. 2012. *Phys. Rev. Lett.* 108(17):178301
121. Hand GL. 1962. *J. Fluid Mech.* 13(01):33–46
122. Phan-Thien N, Mai-Duy N. 2017. *Understanding Viscoelasticity: An Introduction to Rheology*. Graduate Texts in Physics. Cham, Switz.: Springer Int. Publ. AG
123. Goddard J. 2006. *J. Fluid Mech.* 568:1–17
124. Chacko RN, Mari R, Fielding SM, Cates ME. 2018. *J. Fluid Mech.* 847:700–34
125. Ozenda O, Saramito P, Chambon G. 2018. *J. Rheol.* 62(4):889–903
126. Hinch EJ, Leal LG. 1976. *J. Fluid Mech.* 76(1):187–208
127. Phan-Thien N. 1995. *J. Rheol.* 39(4):679–95
128. Gillissen JJJ, Ness C, Peterson JD, Wilson HJ, Cates ME. 2019. *Phys. Rev. Lett.* 123(21):214504
129. Szeri AJ, Leal LG. 1994. *J. Fluid Mech.* 262:171–204
130. Stickel JJ, Phillips RJ, Powell RL. 2007. *J. Rheol.* 51(6):1271–302
131. Ozenda O, Saramito P, Chambon G. 2020. *J. Fluid Mech.* 898:A25
132. Gillissen JJJ, Wilson HJ. 2018. *Phys. Rev. E* 98(3):033119
133. Carreau PJ. 1972. *Trans. Soc. Rheol.* 16(1):99–127
134. Royer JR, Blair DL, Hudson SD. 2016. *Phys. Rev. Lett.* 116(18):188301
135. Nakanishi H, Nagahiro Si, Mitarai N. 2012. *Phys. Rev. E* 85(1):011401
136. Singh A, Mari R, Denn MM, Morris JF. 2018. *J. Rheol.* 62(2):457–68
137. Baumgarten AS, Kamrin K. 2019. *PNAS* 116(42):20828–36
138. Dong J, Trulsson M. 2017. *Phys. Rev. Fluids* 2(8):081301
139. Mari R, Seto R. 2019. *Soft Matter* 15(33):6650–59
140. Jackson R. 1997. *Chem. Eng. Sci.* 52(15):2457–69
141. Deboeuf A, Gauthier G, Martin J, Yurkovetsky Y, Morris JF. 2009. *Phys. Rev. Lett.* 102(10):108301
142. Dbouk T, Lemaire E, Lobry L, Moukalled F. 2013. *J. Non-Newtonian Fluid Mech.* 198:78–95
143. Nott PR, Brady JF. 1994. *J. Fluid Mech.* 275:157–99
144. Nott PR, Guazzelli E, Pouliquen O. 2011. *Phys. Fluids* 23(4):043304
145. Gillissen JJJ, Ness C. 2020. *Phys. Rev. Lett.* 125(18):184503
146. Besseling R, Isa L, Ballesta P, Petekidis G, Cates ME, Poon WCK. 2010. *Phys. Rev. Lett.* 105(26):268301
147. Saint-Michel B, Gibaud T, Manneville S. 2018. *Phys. Rev. X* 8(3):031006
148. Ovarlez G, Le AVN, Smit WJ, Fall A, Mari R, et al. 2020. *Sci. Adv.* 6(16):eaay5589
149. Rathee V, Blair DL, Urbach JS. 2020. *J. Rheol.* 64(2):299–308
150. Leighton D, Acrivos A. 1987. *J. Fluid Mech.* 181:415–39
151. Altobelli SA, Givler RC, Fukushima E. 1991. *J. Rheol.* 35(5):721–34
152. Medhi BJ, Reddy MM, Singh A. 2019. *Adv. Powder Technol.* 30(9):1897–909
153. Balmforth N, Bush J, Craster R. 2005. *Phys. Lett. A* 338(6):479–84
154. Darbois Texier B, Lhuissier H, Forterre Y, Metzger B. 2020. *Commun. Phys.* 3:232

155. Brown E, Jaeger HM. 2012. *J. Rheol.* 56(4):875–923
156. Tang H, Grivas W, Homentcovschi D, Geer J, Singler T. 2000. *Phys. Rev. Lett.* 85(10):2112
157. Eriksen JA, Toussaint R, Måløy KJ, Flekkøy E, Galland O, Sandnes B. 2018. *Phys. Rev. Fluids* 3(1):013801
158. Iveson SM, Litster JD, Hapgood K, Ennis BJ. 2001. *Powder Technol.* 117(1):3–39
159. Cates ME, Wyart M. 2014. *Rheol. Acta* 53:755–64
160. Dagois-Bohy S, Hormozi S, Guazzelli É, Pouliquen O. 2015. *J. Fluid Mech.* 776:R2

Annual Review of Condensed Matter Physics

Volume 13, 2022

Contents

Errata

An online log of corrections to *Annual Review of Condensed Matter Physics* articles may be found at http://www.annualreviews.org/errata/conmatphys